Ligand Binding Shifts Highly Mobile Retinoid X Receptor to the Chromatin-Bound State in a Coactivator-Dependent Manner, as Revealed by Single-Cell Imaging

Peter Brazda, Jan Krieger, Bence Daniel, David Jonas, Tibor Szekeres, Jörg Langowski, Katalin Tóth, Laszlo Nagy and György Vámosi

Mol. Cell. Biol. **2014, 34(7):1234. DOI: 10.1128/MCB.01097-13.**
Published Ahead of Print 21 January 2014.

MCB
Journals.ASM.org

Ligand Binding Shifts Highly Mobile Retinoid X Receptor to the Chromatin-Bound State in a Coactivator-Dependent Manner, as Revealed by Single-Cell Imaging

Peter Brazda,[a,b] Jan Krieger,[d] Bence Daniel,[a] David Jonas,[a,b] Tibor Szekeres,[c] Jörg Langowski,[d] Katalin Tóth,[d] Laszlo Nagy,[a,b] György Vámosi[c]

Department of Biochemistry and Molecular Biology,[a] MTA-DE Lendület Immunogenomics Research Group,[b] and Department of Biophysics and Cell Biology,[c] Research Center for Molecular Medicine, University of Debrecen, Faculty of Medicine, Debrecen, Hungary; German Cancer Research Center, Division Biophysics of Macromolecules, Heidelberg, Germany[d]

Retinoid X receptor (RXR) is a promiscuous nuclear receptor forming heterodimers with several other receptors, which activate different sets of genes. Upon agonist treatment, the occupancy of its genomic binding regions increased, but only a modest change in the number of sites was revealed by chromatin immunoprecipitation followed by sequencing, suggesting a rather static behavior. However, such genome-wide and biochemical approaches do not take into account the dynamic behavior of a transcription factor. Therefore, we characterized the nuclear dynamics of RXR during activation in single cells on the subsecond scale using live-cell imaging. By applying fluorescence recovery after photobleaching and fluorescence correlation spectroscopy (FCS), techniques with different temporal and spatial resolutions, a highly dynamic behavior could be uncovered which is best described by a two-state model (slow and fast) of receptor mobility. In the unliganded state, most RXRs belonged to the fast population, leaving ~15% for the slow, chromatin-bound fraction. Upon agonist treatment, this ratio increased to ~43% as a result of an immediate and reversible redistribution. Coactivator binding appears to be indispensable for redistribution and has a major contribution to chromatin association. A nuclear mobility map recorded by light sheet microscopy-FCS shows that the ligand-induced transition from the fast to the slow population occurs throughout the nucleus. Our results support a model in which RXR has a distinct, highly dynamic nuclear behavior and follows hit-and-run kinetics upon activation.

Transcription is an inherently dynamic process. Paradoxically, most models of transcription factor (TF) behavior assume that TFs are bound to chromatin either permanently or with a fairly long residence time upon activation (seconds to minutes). Recent advances in genomic technologies, such as chromatin immunoprecipitation followed by sequencing (ChIP-Seq), also provided support to such static models (1, 2). However, these methods lack the appropriate time resolution to provide insights into the dynamics of activated transcription factors on the time scale of seconds or shorter.

Nuclear receptors (NRs) can directly bind to DNA via their highly conserved DNA-binding domain (DBD), which is near their N termini. High-affinity binding is made possible by the two zinc finger motifs. This domain recognizes the specific hormone response elements (RE) (3), which are binding sites and/or enhancers regulating transcription of target genes. A consensus RE sequence is AGGTCA (4), which acts as a half site (binds one receptor) for homo- or heterodimer binding. The hinge region of the receptor that gives a high degree of flexibility to the overall structure is located next to the DBD. This part of the protein harbors the nuclear localization signal (NLS) as well. The core of nuclear receptor action lies in the ligand-binding domain (LBD), through which dimer formation, ligand binding, coregulator binding, and *trans* activation occur. Retinoid X receptor (RXR) belongs to the nuclear receptor superfamily and is unique in its ability to act as an obligate heterodimeric partner for many other receptors. The molecular basis of this promiscuous activity is not well understood.

According to the rather static "molecular switch" model, corepressors and members of the repressor complex, including histone deacetylases (HDACs), are bound in the absence of ligand to the NR, which is believed to associate with chromatin (3, 5–8). Upon agonist binding to the LBD, the NR goes through conformation changes. The affinity of the agonist-bound holo form decreases to corepressors and increases to coactivators. As a result, a new set of proteins is bound to the receptor, an activator complex, including histone acetyltransferases (HATs). It is not a far-fetched assumption that coregulator binding has a major effect on chromatin binding, but its contribution to this process is not fully understood.

Recently, ChIP revealed a novel dynamic feature of nuclear receptors. It was found that during estrogen receptor action, unproductive cycles marked by rapid DNA binding alternate with ligand-dependent productive cycles characterized by reduced receptor mobility and longer binding times (9). Fluorescence recovery after photobleaching (FRAP) was among the first methods allowing the study of transcription dynamics by detecting mobility in the subsecond range (10, 11). Such studies represented the

Received 22 August 2013 **Returned for modification** 17 September 2013
Accepted 26 December 2013
Published ahead of print 21 January 2014
Address correspondence to Laszlo Nagy, nagyl@med.unideb.hu.
L.N. and G.V. share senior authorship.
Supplemental material for this article may be found at http://dx.doi.org/10.1128/MCB.01097-13.

doi:10.1128/MCB.01097-13

first challenge to the rigid/static model and led to the proposal of a "hit-and-run" model, which was based on the analysis of variable immobile fractions and half-recovery times of the bleached fluorescence signals of fluorophore-tagged NRs in FRAP experiments (12). Approaches like FRAP ignited interest in studying the kinetics of transcription regulation with greater time resolution. Fluorescence correlation spectroscopy (FCS) utilizes the fluctuation of fluorescence intensity resulting from the diffusion of fluorescently tagged molecules in and out of a confocal (subfemtoliter-sized) volume. With FCS, one can characterize the diffusion properties of molecular subpopulations at millisecond time resolution (13, 14).

We aimed to determine the dynamic properties of the RXR receptor upon ligand activation and integrate results derived from different experimental approaches. Using ChIP-Seq, we found that the genomic regions to which RXR bound were largely the same before and after agonist treatment, but the occupancy of these regions by RXR increased. FRAP showed that ligand activation induced slowing of the half-recovery time, but immobilized receptors were not detected. FCS provided insights into the subsecond range. The diffusion dynamics of the receptors were interpreted by a two-component normal diffusion model representing a fast and a slow component. The slow component most likely represents (transient) DNA binding, which showed a ligand-induced immediate and reversible increase. Importantly, coactivator binding appears to be a major determinant of the shift between the two states.

MATERIALS AND METHODS

Cell culturing, plasmids, and transfection assays. Cell culturing, plasmids, and transfection assays are described in the supplemental material.

ChIP. ChIP was performed as previously described (15), with minor modifications. Briefly, cross-linking was carried out by disuccinimidyl glutarate for 30 min and by formaldehyde (Sigma) treatment for 10 min and was followed by RXR immunoprecipitation. After fixation, chromatin was sonicated with a Diagenode Bioruptor to generate 200- to 1,000-bp fragments. Chromatin was immunoprecipitated with antibodies against preimmune IgG (12-370; Millipore) and RXR (sc-774; Santa Cruz Biotechnologies, Inc.). Chromatin antibody complexes were precipitated with protein A-coated paramagnetic beads (Life Technologies). After 6 washing steps, complexes were eluted and reverse cross-linked. DNA fragments were column purified (MinElute; Qiagen). The amount of immunoprecipitated DNA was quantified with a Qubit fluorometer (Invitrogen). DNA was submitted to quantitative PCR (qPCR) analysis or library preparation. ChIP-seq library preparation and data analysis are described in the supplemental material.

Real-time RT-PCR and immunofluorescence detection. Real-time reverse transcription-PCR (RT-PCR) and immunofluorescence detection are described in the supplemental material.

FRAP. FRAP measurements were performed on an Olympus FluoView 1000 confocal microscope based on an inverted IX-81 stand with an UPlanAPO 60×, 1.2-numeric-aperture (NA) water immersion objective. The 488-nm line of an Ar ion laser excited enhanced green fluorescent protein (EGFP), and emission was detected through a 500- to 550-nm band-pass filter. For quantitative analysis, a 256- by 256-pixel area was selected and scanned with an open pinhole and 10× zoom (pixel size, 82 nm). Before each measurement, 10 prebleach images were taken with 1% laser intensity (9 μW) followed by a 1,500-ms bleach period with 100% laser intensity (900 μW) within the bleach area of 256 by 10 pixels that covered less than 30% of the whole nucleus. Fluorescence pixel intensities of background (outside the cell), region of interest (ROI; i.e., the bleached strip), (the strip), and whole nucleus (the nucleus including the strip but excluding the nucleoli) were determined for each frame with NIH ImageJ v.1.45s. Recovery curves were created, normalized, and evaluated with IGOR software using Phair's double exponential model in the FrapCalc-EMBL module (version V9h).

FCS instrumentation and measurements. FCS measurements were performed on the microscope described above. The 2-channel FCS extension (prototype designed by Jörg Langowski, DKFZ, Heidelberg, Germany) is attached to the 4th detection channel of the confocal scanning unit. FCS measurements on live HeLa cells were performed in 8-well chambered coverglass plates as described above. Fluorescence of EGFP was excited by the 488-nm line of an Ar ion laser, and emission was detected through a 500- to 550-nm band-pass filter by a Perkin-Elmer avalanche photodiode (Perkin-Elmer, Wellesley, MA). Fluorescence autocorrelation curves were calculated online by an ALV-5000E correlator card (ALV-Laser Vertriebsgesellschaft mbH, Langen, Germany). Measurements of 10 8-s runs were taken at three selected points in the nucleus of each selected cell. FCS data acquisition and processing are described in the supplemental material.

SPIM-FCS measurements. Single-plane illumination microscopy (SPIM)-FCS measurements were performed on a custom-built setup described in reference 16. A 491-nm DPSS laser is magnified 5-fold (1× to 8× zoom beam expander) and then relayed (additional ×3 magnification) onto a cylindrical lens (focal length [*f*], 100 mm). An air projection objective (×10 magnification, 0.3 NA; Plan Fluor; Nikon) projects a light sheet into a stainless steel, water-filled sample chamber. Samples are mounted on a motorized XYZ stage. Detection is done using a Nikon CFI Apo-W NIR (×60, 1.0 NA) water-dipping objective. Emitted light is filtered by a 500- to 550-nm band-pass filter. Fluorescent light is imaged onto an iXon X3 860 electron-multiplying charge-coupled device camera (Andor, Belfast, United Kingdom) using a Nikon tube lens (*f*, 200 mm). The camera has a pixel size of 24 by 24 μm^2, corresponding to 400 by 400 nm^2 in the object plane. Adherent HeLa cells were grown on small (~5 by 10 mm^2) pieces of no. 3 coverslips and mounted from above in the sample chamber. The chamber was filled with phenol red-free RPMI medium. Measurements were performed at room temperature (~24°C). SPIM-FCS data acquisition and processing are described in the supplemental material.

RESULTS

Agonist treatment increases genomic binding site occupancy of RXR at the whole-genome level. We first decided to determine the number of binding sites that RXR occupies and the impact of ligand on that in our HeLa-based model system. Chromatin immunoprecipitation followed by next-generation sequencing (ChIP-seq) was performed using HeLa cells treated with a selective RXR agonist (100 nM LG100268) for 1 h. Samples were cross-linked and immunoprecipitated by a pan-RXR antibody. Libraries were generated from the precipitated DNA, which were sequenced and then mapped back to the genome. The genomic locations that showed RXR binding were defined as RXR genomic binding sites. These are typically referred to as peaks, because stacks of short sequences show up as peaks on genome browsers when the data are visualized. Peaks were identified by the Homer2 software. A total of 6,636 genomic regions were determined as binding regions in the control (vehicle-treated) samples. This number increased modestly in the LG268-activated samples, where 8,302 binding sites were detected. A total of 5,138 (more than 50%) of all peaks were identical before and after agonist treatment. These are the sites that appear to be occupied by RXR irrespective of ligand treatment (Fig. 1A). A total of 1,498 sites disappeared, and 3,164 new sites appeared upon activation. The relative position of the two half sites is one important element in the heterodimer selection. Different heterodimers prefer certain direct repeats (DR0 to

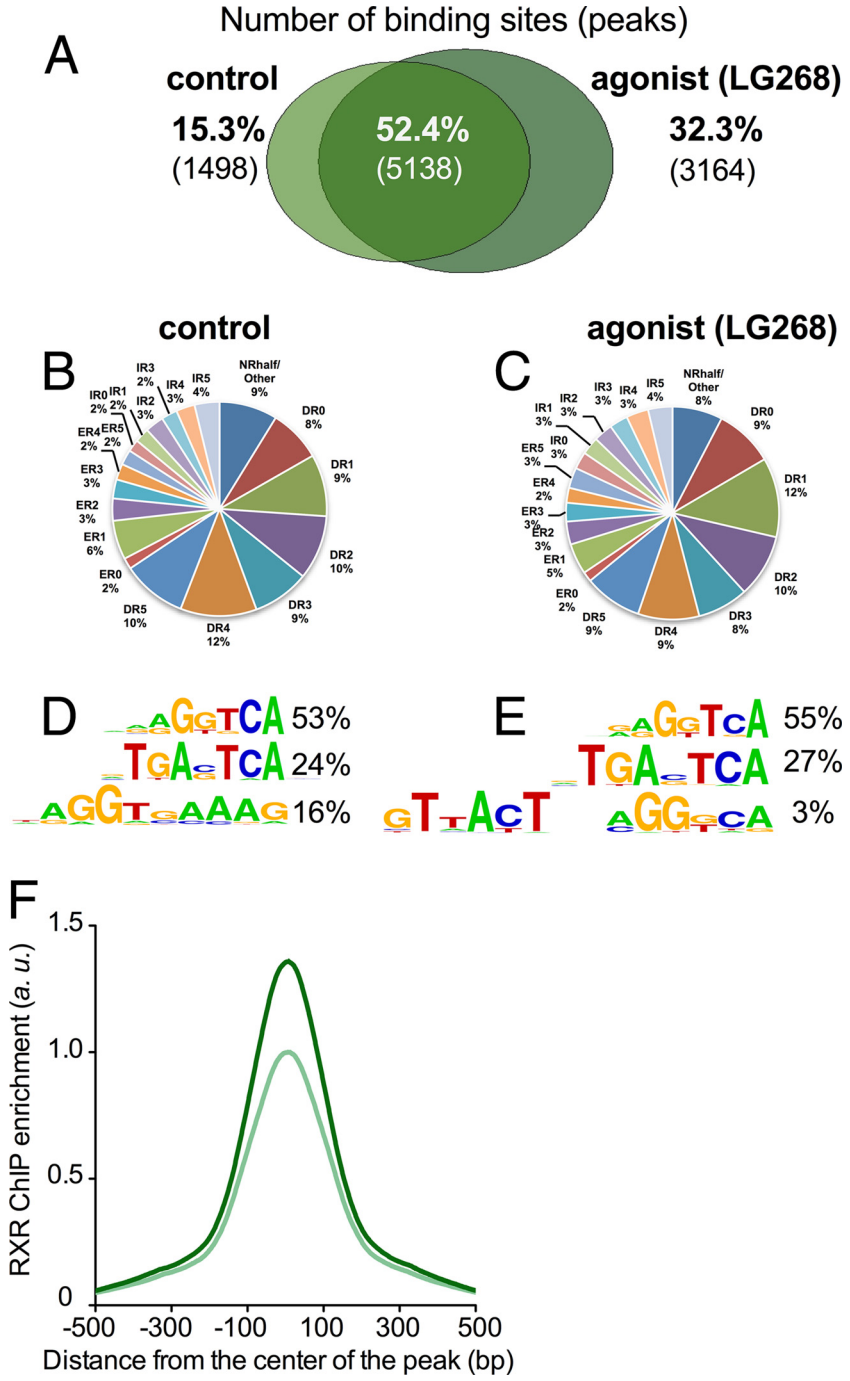

FIG 1 Addition of agonist ligand causes an increase in the probability of chromatin binding. (A) Genomic locations identified as RXR-occupied sites using ChIP-seq in control (vehicle-treated) and agonist (LG268)-treated HeLa cells. The numbers of binding regions determined by Homer2 are plotted. The peak sets of control and LG268-treated samples were compared. The peaks unique for just one state and those common for both states are presented in the Venn diagram. (B and C) Contribution to the different motif sets of NR-binding elements present only in the control sample (B) or only in the LG268-treated sample (C). DR, direct repeat; ER, everted repeat; IR, inverted repeat. Numbers represent the number of spacers between the half-sites of the repeats. (D and E) Motif analysis of the NR binding sites found at the genomic locations shown in panels B and C. The top three motifs are shown according to their strength determined by Homer2. Values next to the motifs represent the fraction of sequences that contained that motif from all of the peaks. (F) Histograms representing the average genome-wide occupancy of RXR binding sites. The ±500 bp flanking the highest peak position of the RXR-binding genomic regions are shown. The binding sites present in both the control- and agonist-treated samples (represented by the intersection of the Venn diagram in panel A) were considered for the presented cumulative peaks. Values are normalized relative to the control data. agonist, LG268 treated.

DR5). The DR, everted repeat (ER), and inverted repeat (IR) preferences of RXR are presented in Fig. 1B (control) and C (LG268 treatment). These diagrams represent the relative distribution of sites occurring only in the control sample (1,498 sites from Fig. 1A) and those occurring exclusively in the LG268-treated sample (3,164 sites from Fig. 1A). Absolute numbers of these sites as well as sites shared by both samples are shown in Fig. S1A in the supplemental material. As expected, DRs are dominant among the identified genomic regions. The distribution of the various DRs did not change upon agonist treatment. Sequence motifs under the peaks (i.e., the genomic locations where RXR was bound) included the consensus AGGTCA half-site sequence of response elements (REs) (Fig. 1D and E). The values in percentages represent the frequency of a motif being detected at the binding site. This value is around 50%, meaning that from all sites where RXR was bound, in 50% of the cases there was a bona fide half-site found. The remaining 50% might include loop formation and tethering/cobinding events with other factors (indirect binding) or direct RXR binding at sites with weaker similarity to the NR half-sites. The distributions of the most frequently found motifs were nearly identical before and after agonist treatment.

Figure 1F shows the histogram of genome-wide distribution of RXR binding sites that are identical before and after agonist treatment (the intersection shown in Fig. 1A). The heights of these cumulative peaks are proportional to the overall probability of RXR being found at the detected genomic locations; therefore, they characterize chromatin occupancy. The maximum tag count number of the peaks increased from 28 to 39 (with mean values from 9.3 to 12, respectively). Thus, within 1 h, ligand activation increased the probability of RXR binding to DNA or chromatin. It is important to emphasize two major issues about this method. First, only bound receptors are detected; because fixation immobilizes receptors on the chromatin, it records an average over the time period of the fixation process of receptor localization. Second, the results obtained here are population averages of millions of cells.

Expression, distribution, and functionality of GFP-tagged RXR. In order to determine the subcellular distribution and expression level of RXR, we studied EGFP-RXR and its truncated form (referred to as GFP-RXR and GFP-RXR-LBD) in HeLa cells using confocal microscopy. GFP-RXR-LBD has the ligand-binding domain but lacks the DNA-binding domain and the NLS. Expression of the full-length construct was tested by Western blotting (see Fig. S2A in the supplemental material). Coregulator binding and transactivation capacity of GFP-fused constructs were documented by luciferase-based transient-transfection assays (see Fig. S2B to D in the supplemental material). Confocal microscopy revealed that full-length GFP-RXR was localized in the nucleus, while GFP-RXR-LBD was distributed homogenously in the cell (Fig. 2A). A cell line stably expressing GFP-RXR was used for further analyses to avoid heterogeneity of the expression level typical for transient transfection. Excessive overexpression could skew binding equilibria of the interacting protein. Therefore, we measured the expression levels in wild-type and GFP-RXR-transfected cells. Real-time quantitative PCR proved that the transfected NRs did not lead to superphysiological levels of expression; the mRNA level of RXR increased ~3-fold (Fig. 2B). The expression level of other tested genes (for retinoic acid receptor α [RARα] ACTR [activator for nucleic acid receptors/SRC-3/NCoA3], and SMRT [silencing mediator of retinoic acid and thyroid hormone receptor/NCoR2]) remained unchanged. We also

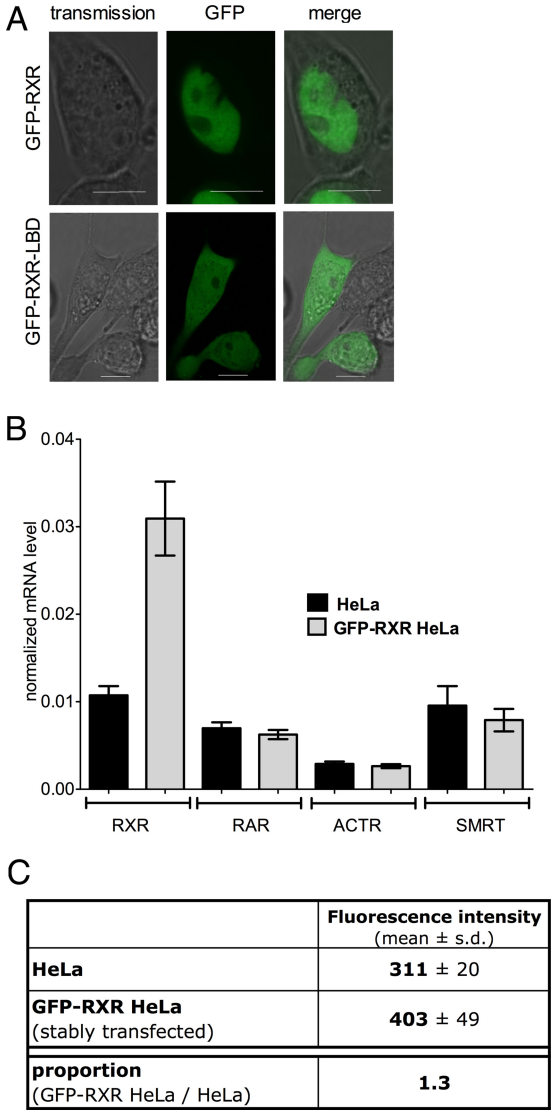

	Fluorescence intensity (mean ± s.d.)
HeLa	**311** ± 20
GFP-RXR HeLa (stably transfected)	**403** ± 49
proportion (GFP-RXR HeLa / HeLa)	**1.3**

FIG 2 Characterization of the HeLa-GFP-RXR cell line. (A) Distribution of GFP-RXR and GFP-RXR-LBD expressed in HeLa cells recorded by live-cell confocal microscopy. Scale bar, 10 μm. (B) mRNA levels of nuclear receptors and cofactors measured by RT-qPCR in the wild-type HeLa cells and HeLa cell line stably expressing GFP-RXR. Results were normalized to the level of human cyclophilin. (C) RXR protein level of wild-type HeLa cells and cells stably transfected with GFP-RXR as detected by immunofluorescence. Intensities were corrected for unspecific binding of the secondary antibody and autofluorescence. s.d., standard deviation.

compared the relative RXR protein expression levels in transfected and wild-type cells by immunofluorescence (Fig. 2C). The ratio was 1.3, indicating that the transfected cells had near-physiological levels of RXR. As usual, this value sets the lower limit of the real expression ratio, because possible unspecific binding of the primary antibody could not be taken into account. The nuclear distribution of endogenous and exogenous (GFP-tagged) RXR was similar in comparisons of immunostained HeLa and HeLa-GFP-RXR cells (see Fig. S3 in the supplemental material). In both cases, homogenous nuclear distribution was observed.

GFP-RXR slows down during activation as determined by FRAP. The intracellular mobility of RXR was studied by FRAP,

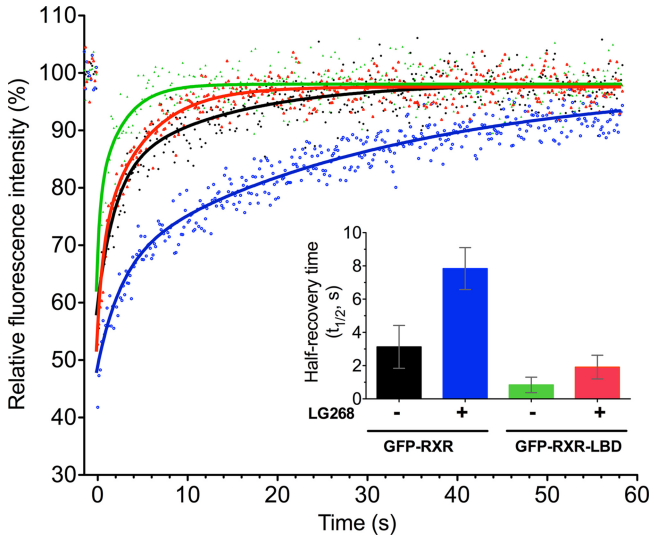

FIG 3 RXR mobility at the minute time scale depends on ligand and DNA binding as revealed by FRAP analysis. Fluorescence recovery curves and half-recovery times of GFP-RXR and GFP-RXR-LBD in the absence (−) and presence (+) of 100 nM LG268. Data are means ± standard deviations. Red bar versus green bar, $P < 0.01$; blue bar versus black bar, $P < 0.001$.

which allows analysis of RXR dynamics on the scale of seconds. The two issues we wished to resolve with this method were (i) whether an immobile fraction appears after ligand treatment and (ii) how the increased DNA-binding probability detected by ChIP-seq is revealed at the single-cell level.

In the absence of ligand, the fluorescence signal in the nuclear ROIs showed rapid recovery after bleaching with a half-recovery time ($t_{1/2}$) of 2.5 ± 0.4 s, and essentially no immobile fraction (3% ± 3%) was detectable. Ten minutes after the addition of 100 nM LG268, the $t_{1/2}$ increased to 7.3 ± 0.7 s, but still no significant immobile fraction was detected (7% ± 3%). Agonist treatment also caused an increase, although to a lesser extent, in the $t_{1/2}$ of GFP-RXR-LBD that lacks direct DNA-binding ability (Fig. 3). In these FRAP experiments, slowing down of RXR was detected during activation, but unlike several other NRs, RXR did not form an immobile fraction that would indicate a longer DNA residence time. This finding agrees with earlier results from different cell lines (17). For these analyses, recovery curves were fitted to a double exponential assuming two diffusing species. The time constants of the components and their fractional amplitudes are shown in Fig. S4 in the supplemental material. In the unliganded state, the fast component of GFP-RXR comprised ~45% of the population, which increased to ~65% upon agonist treatment (see Fig. S4C in the supplemental material). The time constants of both the slow and the fast populations also increased significantly. For GFP-RXR-LBD, both components had significantly shorter time constants than full-length receptors, but a similar increase in the time constants occurred upon agonist treatment. On the other hand, the agonist-induced change of the fractional amplitudes was smaller than that for GFP-RXR.

FCS analysis of RXR mobility at the subsecond scale. To move one step further down the time and distance scales and quantify the mobility parameters of RXR in the millisecond time and submicrometer distance ranges, we applied FCS. We analyzed the fluorescence autocorrelation functions (ACFs) with one- and two-component models of normal and anomalous diffusion (see Fig. S5 and Table S1 in the supplemental material). A single diffusion component with normal diffusion gave a poor fit; introduction of a second component improved the fit significantly. Therefore, we chose the two-component normal diffusion model (Fig. 4A) for representing the data. In the model function, triplet state formation and another slower dark state, due to protonation, were also taken into account (18). Results of anomalous diffusion models are discussed below (see Fig. S5B to E in the supplemental material).

The ranges of the diffusion times were between $\tau_1 = 0.8$ to 3 ms for the fast component and $\tau_2 = 20$ to 120 ms for the slow component (with corresponding diffusion coefficients of $D_1 = 3$ to 12 $\mu m^2/s$ and $D_2 = 0.07$ to 0.5 $\mu m^2/s$) (Fig. 4B, 7th and 9th columns). When these diffusion times were converted into apparent masses [using the Stokes-Einstein relation, $D = kT/(6\pi\eta R)$ for spherical objects and assuming proportionality of molecular mass to R^3, where k is the Boltzmann's constant, T is the absolute temperature, η is viscosity, and R is molecular radius], the slow component gave a 10^6-fold larger mass than the real molecular mass of the GFP-fused nuclear receptor. This difference most likely reflects both an increased molecular mass of the receptor complex and/or the crowded nuclear environment and the interactions of RXR with the chromatin (possibly as part of larger protein complexes). A histogram of the distribution of the diffusion times (Fig. 4C) shows the relative sizes of the two populations and their respective diffusion times (for r_2, 16% of GFP-RXR molecules belong to the slow population, the large majority; for r_1, 84% belong to the fast one). The high fraction of the fast population is not an artifact due to overexpression, as evidenced by the fact that in stably transfected GFP-RXR HeLa cells, neither the diffusion times nor the ratios of the two components depended on the number of molecules in the detection volume (see Fig. S6A to C in the supplemental material). To determine whether the fast population of GFP-RXR consists of freely diffusing molecules, its diffusion time was compared to that of GFP oligomers (Fig. 4B, 1st, 2nd, 3rd, 5th, and 7th columns). The diffusion coefficients of trimeric GFP (with an estimated molecular mass of 81 kDa) and the fast time of GFP-RXR (with an estimated molecular mass of 78 kDa) were similar. From these results, we conclude that the fast population of GFP-RXR diffuses without considerable DNA binding, whereas the slow population interacts with chromatin.

Agonist-dependent changes in RXR mobility are immediate and reversible. RXR plays a central role in nuclear receptor action, forming heterodimers with many different binding partners. The molecular switch model describes receptor-coregulator and receptor-DNA interactions mainly regulated by the agonist ligand. Our question was how ligand-dependent activation and coregulator exchange are reflected in the mobility of RXR. The redistribution of the populations appeared already in the first FCS measurement following activation taken 5 min after the addition of agonist ligand. The ratio of the slow (second) population increased from 16% to 43%, and the distribution of the fast diffusion time shifted to larger values. The mean of the slow diffusion time increased slightly, and its distribution broadened (Fig. 4C). The shift of the related autocorrelation curves is shown in Fig. 4D. To show that this effect is RXR agonist specific, we carried out similar measurements with various agonists of related nuclear receptors. Neither the RARα agonist (AM580) nor the peroxisome proliferator-activated receptor gamma (PPARγ) agonist ligand

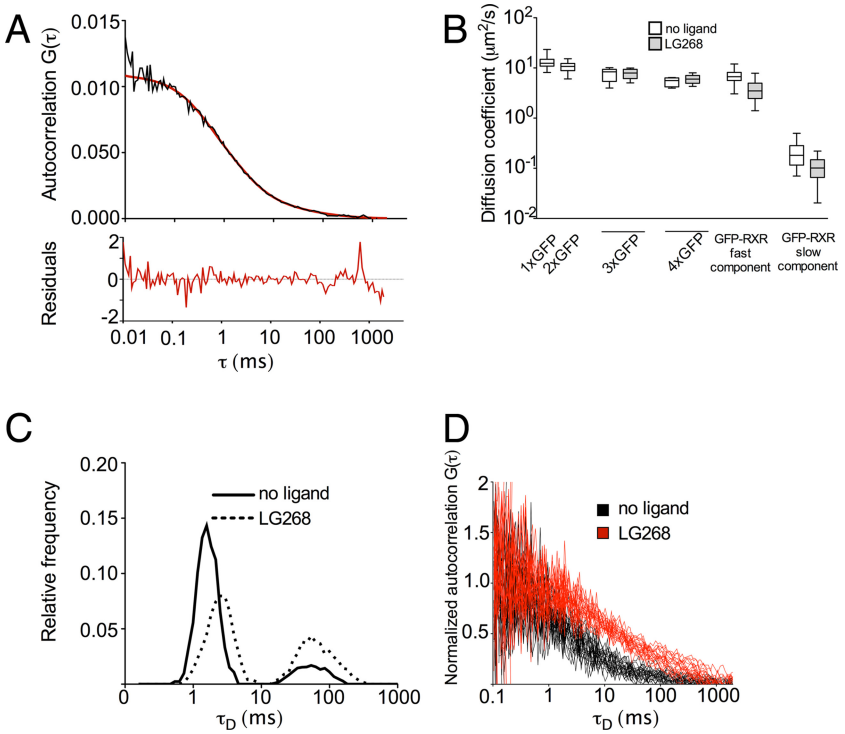

FIG 4 Fraction of the slower population increases rapidly upon agonist treatment according to FCS. (A) Autocorrelation curve [G(τ)] of a representative experiment (black) fitted with the two-component, normal diffusion model (red). τ, lag time. (B) Diffusion coefficients of 1× GFP, 2× GFP, 3× GFP, and 4× GFP (with or without agonist) oligomers fitted with a one-component free-diffusion model compared to the diffusion coefficients of GFP-RXR (with or without agonist) fitted with the two-component normal diffusion model (fast component and slow component). LG268, treatment with 100 nM for 10 min. (C) Distribution of diffusion times (τ_D) of GFP-RXR before (no ligand) and 10 min after (LG268) the addition of 100 nM LG268. (D) Normalized autocorrelation curves of a representative experiment ($n > 30$).

(rosiglitazone) caused an increase in the size of the slow population (r_2); only ligands described as RXR agonists (LG268 and 9-*cis* retinoic acid) did (Fig. 5A). As an attempt to reveal the kinetics of the effect, we carried out a time-lapse experiment. The effect was detectable already at our first time point (4 min) (Fig. 5B). The effect was dose dependent (Fig. 5C). Based on these and earlier, luciferase assay-based activation measurements, we decided to apply LG268 agonist at a 100 nM concentration. To rule out an agonist-dependent global viscosity change of the nucleus, we compared the diffusion coefficients of 3× GFP and 4× GFP with or without LG268. Diffusion coefficients of all the GFP-related experiments are summarized in Fig. 4B. The GFP oligomers showed no change in their diffusion, which implies that ligand-induced effects were specific for RXR. Confocal images of the distribution of GFP oligomers and GFP-RXR with or without ligand treatment are shown in Fig. S7A in the supplemental material.

We found earlier that the agonist-dependent redistribution of RAR (a heterodimer partner of RXR) was not reverted when the ligand was removed from the medium (13), implying a low off-rate in the receptor-chromatin interaction. In contrast to RAR, the redistribution of the two RXR populations was reverted completely when the agonist was removed from the medium (Fig. 5A, last column). This experiment was repeated using 9-*cis* retinoic acid and gave the same result, indicating that the agonist effect was reversible (Fig. 5D). Interestingly, transition to the slow state occurred repeatedly after a second ligand treatment (last column).

Coactivator binding has a large impact on the diffusion of activated RXR. NRs directly connect extra- and intracellular signals with the chromatin through protein-ligand, protein-DNA, and protein-protein interactions. Studying the effect of coregulator binding on the mobility of RXR in live cells provides crucial information on NR action in the framework of the molecular switch model. Thus, we fused the interaction domains (ID) of either the SMRT corepressor or the ACTR coactivator to a consensus nuclear localization signal and an mCherry fluorophore (mCherry-NLS-SMRT-ID/repressor peptide and mCherry-NLS-ACTR-ID/activator peptide). The expressed peptides can still recognize and bind RXR but lack the domain necessary for binding additional members of the large coregulator complexes. As such, they act as competitive inhibitors of endogenous coregulator complexes by preventing full-length coregulators and additional members of the complex from binding there. One or the other short peptide was cotransfected along with GFP-RXR, the diffusion of which was then measured (Fig. 6A). Expression levels of the tagged proteins were monitored via their fluorescence signal. With no ligand added, cotransfection of the ID peptides did not change the size of the fraction of the slower population. Treatment with LG268 in the presence of the repressor peptide caused a transition to the slow state similar to that observed earlier. On the other hand, no ligand-induced redistribution occurred when the activator peptide was cotransfected (last column). The presence of the exogenous activator IDs prevented endogenous coactivator binding; thus, the slowing down of RXR could not take place. This

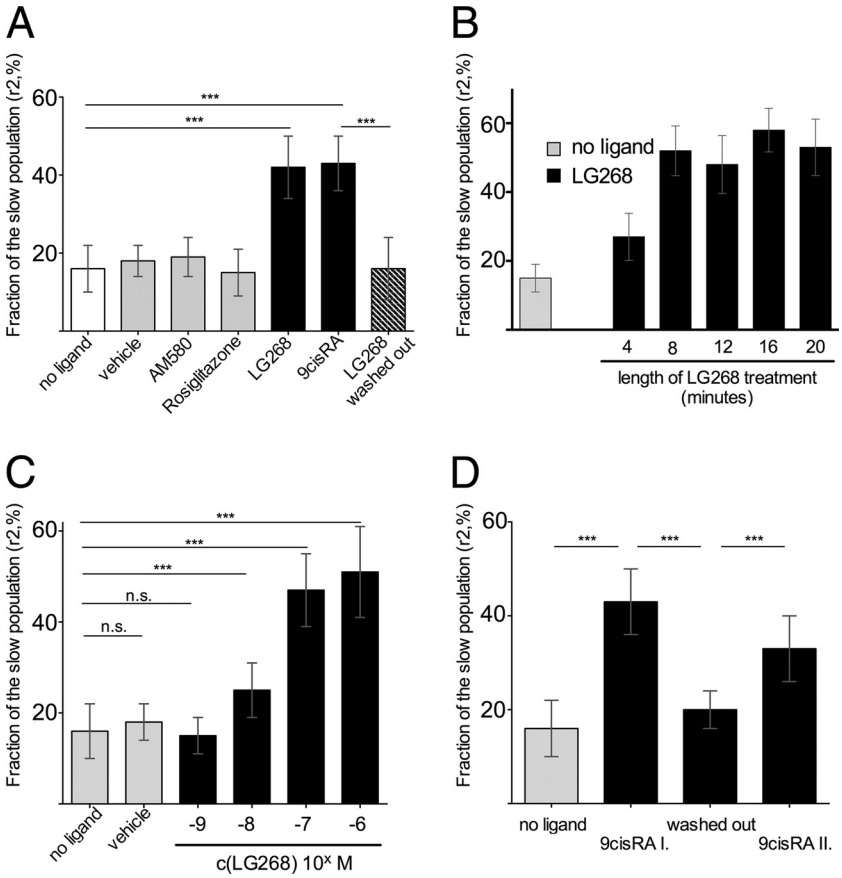

FIG 5 Characterization of the effect of LG268 on the diffusion of GFP-RXR according to FCS. (A) Fraction of the slow population (r_2) before and 10 min after addition of vehicle or 100 nM AM580, rosiglitazone, LG268, or 9-*cis* retinoic acid or after the replacement of the LG268-containing medium with the vehicle-containing one. Data are means ± standard deviations. (B) Fraction of the slow population (r_2) before and 4, 8, 12, 16, and 20 min after addition of 100 nM LG268. (C) Fraction of the slow population (r_2) before or 10 min after addition of (10^{-9} to 10^{-6} M) LG268. (D) Fraction of the slow population (r_2) before and 10 min after addition of 100 nM 9-*cis* retinoic acid, after the replacement of the 9-*cis* retinoic acid-containing medium with the vehicle-containing one, and after the second 9-*cis* retinoic acid administration. ***, $P < 0.001$ in all panels; n.s., not significant.

phenomenon fits well in our general concept of NRs, where the main event of activation is the binding of the activator complex. The repressor peptide was displaced by the coactivator complex upon ligand binding; thus, RXR slowed down. However, formation of coactivator complexes was probably blocked via competitive inhibition by the activator peptides, implying that binding of full-length coactivator is essential for the ligand-dependent slowing down of RXR. This also means that the chromatin-binding affinity of the receptor in the activator complex is larger than in the absence of ligand (when the receptor is either in a repressor complex or diffuses freely).

The effect of coactivator binding on RXR mobility was tested in another set of experiments as well. LG1208 is a synthetic (RXRα-specific) ligand that acts as a competitive antagonist (19, 20). Its effect was tested in the mammalian two-hybrid system, where the affinity of RXR to coregulators was measured in the presence or absence of ligands. LG1208 did not significantly alter the corepressor binding ability of RXR (see Fig. S8 in the supplemental material); however, unlike an agonist ligand, it failed to enhance the coactivator binding affinity of RXR. In a dual-ligand treatment, LG1208 diminished the LG268 effect when it was applied in 10-fold excess (see Fig. S8B). Summing these effects up, we assume that LG1208 occupies the ligand-binding pocket of the receptor, which induces a conformation of RXR incompatible with coactivator binding. These findings were corroborated by FCS measurements. The antagonist alone did not change r_2, but in combination with the agonist ligand (LG268 plus LG1208), it prevented the agonist-induced redistribution (Fig. 6B). This supports our finding that coactivator binding is a prerequisite for the mobility shift of RXR.

Direct DNA binding has a smaller impact on RXR mobility than indirect DNA binding or coactivator binding. Due to the fact that RXR is a transcription factor, one of its key characteristics is direct DNA binding. Therefore, we expected that abolishing the DNA binding affinity of the receptor would have a major effect on its diffusion. A truncated form of the receptor that contains only the LBD (i.e., lacking the DBD) was fused to GFP (GFP-RXR-LBD). Our FRAP measurements already showed that this truncated form had a substantially higher mobility than the full-length receptor, still it responded to activation with an increased half-recovery time (Fig. 3). This mutant is still capable of ligand and coregulator binding and dimer formation but is unable to bind to DNA directly. It is important to emphasize, though, that DNA binding of the GFP-RXR-LBD construct via the (full-length, endogenous) dimer partners of RXR cannot be excluded. The FCS measurements in the nucleus showed a slightly shorter diffusion

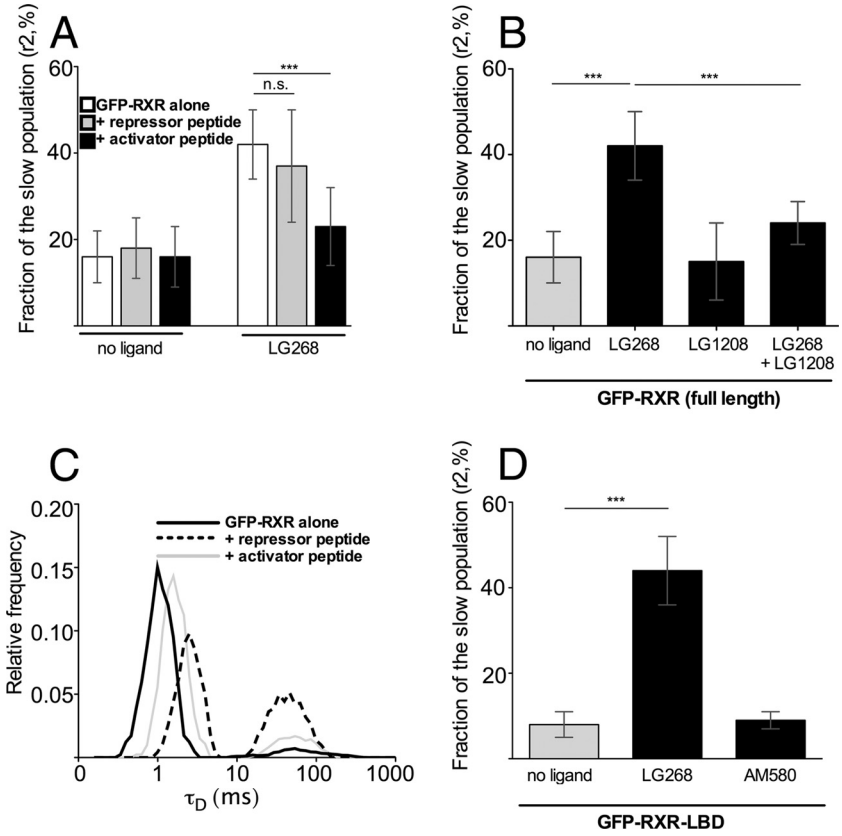

FIG 6 Coactivator binding and direct or indirect DNA binding is needed for the agonist-induced slowing of RXR. (A) FCS-derived fractions of the slow population (r_2) of GFP-RXR alone or with the cotransfection of a repressor peptide (mCherry-NLS-SMRT-ID1+2) or an activator peptide (mCherry-NLS-ACTR-ID1+2) before no ligand and 10 min after the addition of 100 nM LG268. Data are means ± standard deviations. ***, $P < 0.001$ for all panels. (B) FCS-derived fractions of the slow population (r_2) of GFP-RXR before and 10 min after the addition of 100 nM LG268, the addition of 1 μM LG1208 (antagonist), and the coadministration of the two. (C) Distributions of diffusion times of GFP-RXR-LBD molecules before (GFP-RXR alone) and 10 min after (+ repressor peptide) the addition of 100 nM LG268 are shown and are compared to the wild-type form (+ activator peptide). (D) FCS-derived fractions of the slow population (r_2) of GFP-RXR-LBD before and 10 min after the addition of 100 nM LG268 or 100 nM AM580 (RAR agonist).

time for the fast population than GFP-RXR (Fig. 6C). This can be related to the smaller molecular mass of the truncated receptor. The apparent diffusion time of the slow component did not differ significantly from that of GFP-RXR, but its fraction (<10%) was smaller than that of the full-length form. This difference in the slow fractions implies that DNA binding or chromatin association occurs in the unliganded state of the full-length RXR, in accordance with its role in corepressor complexes. Interestingly, as the agonist was added to the transfected cells, the slow fraction of GFP-RXR-LBD changed similarly to the full-length receptor; r_2 increased to 40% (Fig. 6D). According to our FCS measurements, direct DNA binding influences the mobility of RXR; however, probably due to its numerous interacting partners (receptors and coregulators), coactivator (and probably indirect DNA binding) binding is the essential element for the slowing down during activation.

Parallel mobility measurements by SPIM-FCS reveal that RXR's dynamic properties are similar throughout the nucleus during activation. Finally, to visualize the spatial distribution of the mobility of RXR and the effect of activation, we used single-plane illumination microscopy FCS (SPIM-FCS). The advantage of single-plane illumination with detection in the entire image plane is that not just one but a whole set (up to 40 by 20) of FCS autocorrelation functions can be determined simultaneously in a single experiment. By fitting these curves, a nuclear mobility map of RXR can be constructed. As shown in Fig. 7, the fraction of the slowly diffusing RXR increased after LG268 treatment in the full-length as well as in the LBD form. In most cells, the localization of GFP-RXR-LBD changed upon ligand treatment: the initially homogeneous distribution was replaced by a more pronounced nuclear localization. As presented in the mobility map of the slow component, the unliganded state of the truncated form had a small slow population. As LG268 was applied, the slow population increased. Thus, the redistribution detected by FCS was confirmed and refined by SPIM-FCS. In addition, it was revealed that the distribution of populations appeared rather homogenous; no nuclear architecture related pattern could be recognized either before or after activation.

DISCUSSION

Genome-wide methods refine our models and understanding of transcription factor action. NRs contribute to signal transduction by directly connecting lipid mediator levels and gene expression. Their structures allow them to interact with different ligand molecules, regulatory proteins, and the DNA at the same time, making them ideal regulatory tools. However, their dynamic be-

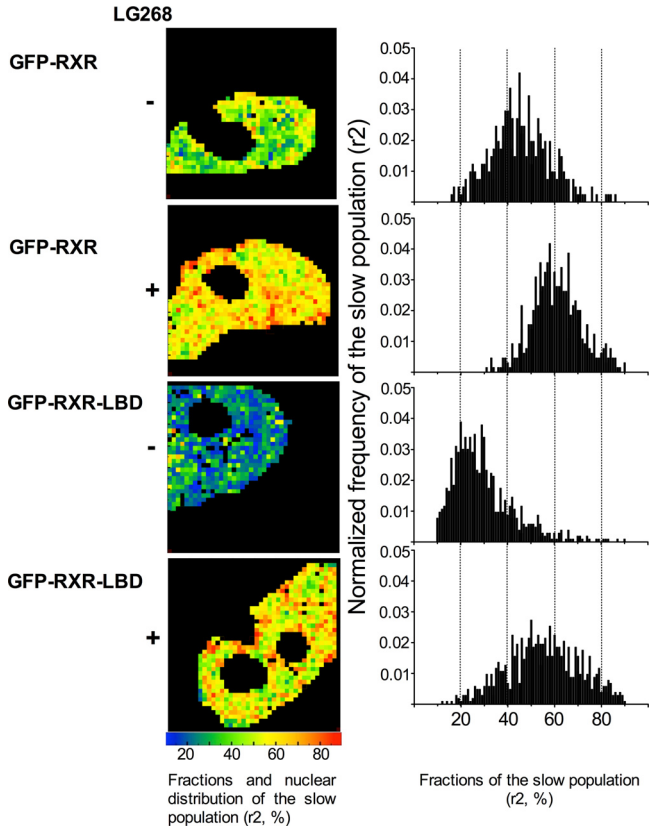

FIG 7 SPIM-FCS reveals a homogenous ligand-induced transition of RXR to the slow state in the entire nucleus. Cellular map of the fraction of the slow population (r_2) of GFP-RXR and GFP-RXR-LBD in the absence and presence of ligand. Diagrams display the full range of r_2 in the presented cells.

havior upon activation is not well characterized. Many of the NRs' interactions have been extensively studied. The identity of the interacting partners and potential ligands may be tested by various two-hybrid studies, and transfection-based assays identified response elements. Their function can be analyzed using electrophoretic mobility shift assay (EMSA) and enhancer/trap experiments.

These *in vitro* biochemical approaches provide information about the steady state, and they average the observed activity of millions of cells. However, cellular processes, especially transcription, are very dynamic. Very often a protein spends most of its time in low-affinity interactions with elements of the genome rather than binding to its specific sites, which results in a highly mobile and dynamic system (21, 22).

ChIP experiments (9, 23–25) raised the possibility that TF populations with different dynamic properties could coexist, representing rapid DNA binding-unbinding (detectable by FRAP) and long-term engagement (referred to as productive engagement) on a promoter along with other TF partners, resulting in slower mobility (detected by ChIP).

An enigma in understanding TF dynamics is still the connection between biochemical and genome-wide assays on the one hand and between genome-wide and single-cell assays on the other. Here, we studied the effects of transcriptional activation on RXR's behavior at different spatial and temporal resolutions. ChIP coupled with high-throughput sequencing enabled us to identify the DNA binding regions at the whole-genome scale. The overall number of RXR-occupied sites increased upon ligand activation. Analysis of the genome-wide distribution of RXR binding sites revealed an increase in the probability of RXR being bound to these DNA elements, resulting in increased occupancy after activation. These experiments provided a population and time average of the changes during RXR activation, as millions of cells were processed together. To study the observed affinity change in more detail and with a better time resolution, we applied fluorescence microscopy methods, which also allow single-cell detection.

From genome-wide to single cell. According to previous FRAP measurements, NRs can be divided into two groups based on their response to activation. Androgen receptor (26) and estrogen receptor (27) become immobile after activation, while no immobile fraction appears in the case of glucocorticoid receptor (28), PPAR, vitamin D receptor (29), RAR, and RXR (30, 31). We confirmed the latter result in our model system. No long-term RXR binding was detectable, but a clear increase in recovery time was detectable on the time scale of seconds, corresponding to the slowing down of diffusion on the micrometer scale. The ligand-dependent change in recovery time was also seen when the DBD of the receptor was removed, rendering it unavailable for direct DNA binding. This led us to investigate whether interactions other than those between DNA and the receptor significantly affect RXR mobility.

By applying FCS we achieved a time resolution of milliseconds. FCS with other NRs and DNA binding proteins showed that models with either one-component anomalous diffusion (PPAR [32]) or two-component normal diffusion (HP1 [33], RAR [13], Fos-Jun [34, 35]) could fit the data. This ambiguity more likely reflects the limitations of the method rather than the diversity of NR action.

FCS fit models attempt to describe the dynamics of a multicomponent system. Even an inert macromolecule such as GFP exhibits anomalous diffusion, with an anomaly parameter (α) of ~0.85 inside the nucleus (36–38) or in solution packed with macromolecules (39). Macromolecules that interact with multiple other species most probably exist in various states with different mobility, contrary to what a one-component model assumes. In our system, RXR showed the best fit with at least two diffusion components, meaning that at least two distinct populations of RXR could be distinguished based on their mobility by FCS. Although a two-component anomalous diffusion model fits the data slightly better, the values of the fit parameters become more uncertain without changing the most important conclusions. The major effect discussed in this study, the slowing down of receptor diffusion upon ligand binding, can be identified in each model.

The first, mobility maps of fluorescent tracer proteins in live cell nuclei were obtained by Dross et al. (36). Single-plane illumination fluorescence correlation spectroscopy (SPIM-FCS) probes in homogeneous three-dimensional environments (40–43), enabling the simultaneous measurement of mobility in two-dimensional sections of whole nuclei. The diffusion parameters (diffusion coefficients and fractions of the populations) determined by imaging FCS measurements showed a good match with those of single-point confocal FCS measurements. Diffusion maps also revealed that there were no distinct patterns of RXRs with different diffusion coefficients. This suggested that liganded RXR was not enriched in so-called transcription factories.

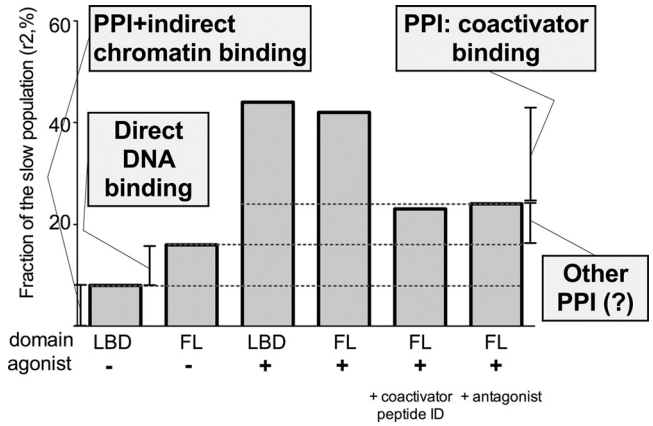

FIG 8 Simplified model of the contribution of protein-protein and protein-DNA interactions to the formation of the slow fraction of GFP-RXR. PPI, protein-protein interaction; FL, full-length receptor (GFP-RXR); LBD, ligand binding domain (GFP-RXR-LBD). Comparison of the values of r_2 for the LBD and the full-length receptor in the absence of ligand shows the importance of DNA binding for the formation of the slow fraction, which is larger for the full-length receptor (first two columns). Ligand activation greatly increases overall DNA binding, which may be direct or indirect via the DBD of the dimeric receptor partner (3rd and 4th columns). This increase is impaired if binding of the full-length coactivator is competed off by the short coactivator fragment (ACTR ID) or by an antagonist ligand (last two columns).

A refined model of RXR action. Based on these analyses, we suggest here a refined model of the contribution of the various interactions to RXR dynamics (Fig. 8). The slowly diffusing population of RXR in the absence of ligand implies direct binding to DNA or chromatin. Loss of the DBD results in a significant decrease of this population. The remaining slow population may represent the effect of protein-protein interactions or indirect DNA binding via its dimer partners (Fig. 8, first column). When direct DNA binding is present (full-length receptor), the fraction of the slow population increases due to protein-DNA interactions, although it still remains a minor part of the total. This stage might represent the scanning motion of NRs when they bind to many different regions of the genome for short periods of time (Fig. 8, second column). As agonist appears, RXR changes into its ligand-bound conformation, which has an increased coregulator binding affinity compared to that of the unliganded conformation. Response element-specific DNA binding and coactivator binding becomes stronger at this stage (Fig. 8, third and fourth columns). DNA-RXR interactions probably last longer in this state, but for the full effect (expansion of the slow state) to take place, binding of coactivators and further components of the activator complex seems essential. Surprisingly, this effect also occurs in the absence of direct DNA binding ability, probably due to the interactions between RXR and the activator complex (which includes proteins with direct DNA binding capacity, most probably via the heterodimeric receptor partner). This aspect of our model is based on the inhibition experiments in FCS measurements (with the short coregulator ID peptides) and the effect of the LG1208 antagonist on the formation of the coactivator bound state of RXR (Fig. 8, fifth and sixth columns). When full-length coactivator binding is inhibited in the system, the fraction of the slow population of RXR drops to nearly the level of the non-ligand-bound state. The difference between this state and the non-ligand-bound state (Fig. 8, second column) might be either the result of incomplete competition during our measurements or forced dimer formation due to the presence of the agonist ligand (and the peptide ID binding to both RXR and RAR).

An interesting aspect of NR activation is that ligand binding and ligand-induced DNA binding seem to be uncoupled in a certain sense. When activating RAR-LBD with the specific ligand of RAR, we got results similar to those described here for RXR-LBD: the slow fraction of RAR-LBD increased (13). This suggests that ligand binding at either side of an NR dimer induces the binding of activator, and the consequent enhancement of DNA binding can be due to the nonactivated side as well; in other words, ligand binding and DNA binding can be performed by two distinct components of a dimer.

A comparison sheds some light on the difference between RAR, which has only one potential partner, and RXR, which is available for many partners and takes part in many interactions. Compared to RXR, RAR had a larger fraction in the slow state in the absence of ligand, its ligand-induced increase was less (only 15%), and, contrary to the case of RXR, the change persisted even after washing out the ligand (13). Moreover, the specific ligands of neither RXR nor RAR had any significant effect on the mobility of the other receptor. Our interpretation of these differences is that protein-protein interactions and DNA binding are looser and more flexible in the case of the promiscuous RXR than for RAR. In addition, the two receptors may move partially independently from each other and not necessarily as heterodimers.

Immediate and specific response to various types of stimuli requires a dynamic system. This is known for several nuclear proteins, but the presence of a high mobility state at different time scales had not been demonstrated for the master regulator of NR action, RXR. According to our results, compared to RAR, the mobility of RXR covers a wider range and its activation-induced changes are more transient. This flexibility and large dynamic range fits well with the role of RXR as a promiscuous partner. Its carrier-like behavior, providing a docking surface for coregulators and regulatory complexes, makes continuous availability important. This can be achieved if the transient nature of ligand and DNA binding is added to the hit-and-run model.

The exact cause of anomalous nuclear diffusion is still an open question. It should be mentioned that the anomaly parameter of the slower component of RXR (in the case of using the two-component anomalous diffusion model) showed superdiffusion ($\alpha > 1$) (see Fig. S2E and F and Table S1 in the supplemental material). This could be the reflection of short-range directed diffusion of RXR scanning through the available DNA elements with nonspecific binding or a locally directed "flow" of chromatin segments together with the bound receptor. Because SPIM-FCS offers the possibility of measuring directed flow through pixel-pixel cross-correlation analysis, it might offer answers to this question by providing high-resolution pictures of the receptor's activity in the nuclei of single cells.

The model emerging from these studies is rather dynamic and compatible with a "hit-and-run," or rather "scan-and-stop," scenario in which RXR's nuclear mobility is dependent principally on coactivator, receptor, and chromatin binding.

ACKNOWLEDGMENTS

We acknowledge Monika Fuxreiter and members of the Nagy laboratory for discussions and comments on the manuscript. We thank Ibolya Furtos, Beata Szalka, and Marta Beladi for technical assistance. The genome

sequence used in this research was derived from a HeLa cell line. Henrietta Lacks and the HeLa cell line that was established from her tumor cells in 1951 have made significant contributions to scientific progress. We are grateful to Henrietta Lacks, now deceased, and to her surviving family members for their contributions to biomedical research.

This work was supported by grants from the Hungarian Scientific Research Fund (OTKA K100196 to L.N.; K77600 and K103965 to G.V.), a grant from the Magyar Ösztöndíj Bizottság and the Deutscher Akademischer Austausch Dienst (MÖB/21-1/2013 to G.V. and K.T.), and TÁMOP-4.2.2.A-11/1/KONV-2012-0023 VÉDELEM implemented through the New Hungary Development Plan, cofinanced by the European Social Fund and the European Regional Development Fund (to L.N.). This research was supported by the European Union and the State of Hungary, cofinanced by the European Social Fund in the framework of the TÁMOP-4.2.4.A/2-11/1-2012-0001 National Excellence Program (to G.V.).

REFERENCES

1. **Delacroix L, Moutier E, Altobelli G, Legras S, Poch O, Choukrallah MA, Bertin I, Jost B, Davidson I.** 2010. Cell-specific interaction of retinoic acid receptors with target genes in mouse embryonic fibroblasts and embryonic stem cells. Mol. Cell. Biol. **30:**231–244. http://dx.doi.org/10.1128/MCB.00756-09.
2. **Reddy TE, Pauli F, Sprouse RO, Neff NF, Newberry KM, Garabedian MJ, Myers RM.** 2009. Genomic determination of the glucocorticoid response reveals unexpected mechanisms of gene regulation. Genome Res. **19:**2163–2171. http://dx.doi.org/10.1101/gr.097022.109.
3. **Mangelsdorf DJ, Evans RM.** 1995. The RXR heterodimers and orphan receptors. Cell **83:**841–850. http://dx.doi.org/10.1016/0092-8674(95)90200-7.
4. **Glass CK.** 1994. Differential recognition of target genes by nuclear receptor monomers, dimers, and heterodimers. Endocrine Rev. **15:**391–407. http://dx.doi.org/10.1210/edrv-15-3-391.
5. **Chen JD, Evans RM.** 1995. A transcriptional co-repressor that interacts with nuclear hormone receptors. Nature **377:**454–457. http://dx.doi.org/10.1038/377454a0.
6. **Love JD, Gooch JT, Benko S, Li C, Nagy L, Chatterjee VK, Evans RM, Schwabe JW.** 2002. The structural basis for the specificity of retinoid-X receptor-selective agonists: new insights into the role of helix H12. J. Biol. Chem. **277:**11385–11391. http://dx.doi.org/10.1074/jbc.M110869200.
7. **Mangelsdorf DJ, Thummel C, Beato M, Herrlich P, Schutz G, Umesono K, Blumberg B, Kastner P, Mark M, Chambon P, Evans RM.** 1995. The nuclear receptor superfamily: the second decade. Cell **83:**835–839. http://dx.doi.org/10.1016/0092-8674(95)90199-X.
8. **Nagy L, Kao HY, Love JD, Li C, Banayo E, Gooch JT, Krishna V, Chatterjee K, Evans RM, Schwabe JW.** 1999. Mechanism of corepressor binding and release from nuclear hormone receptors. Genes Dev. **13:**3209–3216. http://dx.doi.org/10.1101/gad.13.24.3209.
9. **Metivier R, Reid G, Gannon F.** 2006. Transcription in four dimensions: nuclear receptor-directed initiation of gene expression. EMBO Rep. **7:**161–167. http://dx.doi.org/10.1038/sj.embor.7400626.
10. **Sprague BL, McNally JG.** 2005. FRAP analysis of binding: proper and fitting. Trends Cell Biol. **15:**84–91. http://dx.doi.org/10.1016/j.tcb.2004.12.001.
11. **van Royen ME, Farla P, Mattern KA, Geverts B, Trapman J, Houtsmuller AB.** 2009. Fluorescence recovery after photobleaching (FRAP) to study nuclear protein dynamics in living cells. Methods Mol. Biol. **464:**363–385. http://dx.doi.org/10.1007/978-1-60327-461-6_20.
12. **Gelman L, Feige JN, Tudor C, Engelborghs Y, Wahli W, Desvergne B.** 2006. Integrating nuclear receptor mobility in models of gene regulation. Nuclear Receptor Signal. **4:**e010. http://dx.doi.org/10.1621/nrs.04010.
13. **Brazda P, Szekeres T, Bravics B, Toth K, Vamosi G, Nagy L.** 2011. Live-cell fluorescence correlation spectroscopy dissects the role of coregulator exchange and chromatin binding in retinoic acid receptor mobility. J. Cell Sci. **124:**3631–3642. http://dx.doi.org/10.1242/jcs.086082.
14. **Hendrix J, Gijsbers R, De Rijck J, Voet A, Hotta J, McNeely M, Hofkens J, Debyser Z, Engelborghs Y.** 2011. The transcriptional co-activator LEDGF/p75 displays a dynamic scan-and-lock mechanism for chromatin tethering. Nucleic Acids Res. **39:**1310–1325. http://dx.doi.org/10.1093/nar/gkq933.
15. **Barish GD, Yu RT, Karunasiri M, Ocampo CB, Dixon J, Benner C, Dent Tangirala ALRK, Evans RM.** 2010. Bcl-6 and NF-kappaB cistromes mediate opposing regulation of the innate immune response. Genes Dev. **24:**2760–2765. http://dx.doi.org/10.1101/gad.1998010.
16. **Singh AP, Krieger JW, Buchholz J, Charbon E, Langowski J, Wohland T.** 2013. The performance of 2D array detectors for light sheet based fluorescence correlation spectroscopy. Optics Express **21:**8652–8668. http://dx.doi.org/10.1364/OE.21.008652.
17. **Dong S, Stenoien DL, Qiu J, Mancini MA, Tweardy DJ.** 2004. Reduced intranuclear mobility of APL fusion proteins accompanies their mislocalization and results in sequestration and decreased mobility of retinoid X receptor alpha. Mol. Cell. Biol. **24:**4465–4475. http://dx.doi.org/10.1128/MCB.24.10.4465-4475.2004.
18. **Haupts U, Maiti S, Schwille P, Webb WW.** 1998. Dynamics of fluorescence fluctuations in green fluorescent protein observed by fluorescence correlation spectroscopy. Proc. Natl. Acad. Sci. U. S. A. **95:**13573–13578. http://dx.doi.org/10.1073/pnas.95.23.13573.
19. **Wallen-Mackenzie A, Mata de Urquiza A, Petersson S, Rodriguez FJ, Friling S, Wagner J, Ordentlich P, Lengqvist J, Heyman RA, Arenas E, Perlmann T.** 2003. Nurr1-RXR heterodimers mediate RXR ligand-induced signaling in neuronal cells. Genes Dev. **17:**3036–3047. http://dx.doi.org/10.1101/gad.276003.
20. **Lengqvist J, Mata De Urquiza A, Bergman AC, Willson TM, Sjovall J, Perlmann T, Griffiths WJ.** 2004. Polyunsaturated fatty acids including docosahexaenoic and arachidonic acid bind to the retinoid X receptor alpha ligand-binding domain. Mol. Cell. Proteomics **3:**692–703. http://dx.doi.org/10.1074/mcp.M400003-MCP200.
21. **Hager GL, McNally JG, Misteli T.** 2009. Transcription dynamics. Mol. Cell **35:**741–753. http://dx.doi.org/10.1016/j.molcel.2009.09.005.
22. **Carlberg C, Seuter S.** 2010. Dynamics of nuclear receptor target gene regulation. Chromosoma **119:**479–484. http://dx.doi.org/10.1007/s00412-010-0283-8.
23. **George AA, Schiltz RL, Hager GL.** 2009. Dynamic access of the glucocorticoid receptor to response elements in chromatin. Int. J. Biochem. Cell Biol. **41:**214–224. http://dx.doi.org/10.1016/j.biocel.2008.09.019.
24. **Hager GL, Nagaich AK, Johnson TA, Walker DA, John S.** 2004. Dynamics of nuclear receptor movement and transcription. Biochim. Biophys. Acta **1677:**46–51. http://dx.doi.org/10.1016/j.bbaexp.2003.09.016.
25. **Voss TC, Schiltz RL, Sung MH, Yen PM, Stamatoyannopoulos JA, Biddie SC, Johnson TA, Miranda TB, John S, Hager GL.** 2011. Dynamic exchange at regulatory elements during chromatin remodeling underlies assisted loading mechanism. Cell **146:**544–554. http://dx.doi.org/10.1016/j.cell.2011.07.006.
26. **Farla P, Hersmus R, Geverts B, Mari PO, Nigg AL, Dubbink HJ, Trapman J, Houtsmuller AB.** 2004. The androgen receptor ligand-binding domain stabilizes DNA binding in living cells. J. Struct. Biol. **147:**50–61. http://dx.doi.org/10.1016/j.jsb.2004.01.002.
27. **Stenoien DL, Patel K, Mancini MG, Dutertre M, Smith CL, O'Malley BW, Mancini MA.** 2001. FRAP reveals that mobility of oestrogen receptor-alpha is ligand- and proteasome-dependent. Nat. Cell. Biol. **3:**15–23. http://dx.doi.org/10.1038/35050515.
28. **Schaaf MJ, Cidlowski JA.** 2003. Molecular determinants of glucocorticoid receptor mobility in living cells: the importance of ligand affinity. Mol. Cell. Biol. **23:**1922–1934. http://dx.doi.org/10.1128/MCB.23.6.1922-1934.2003.
29. **Prufer K, Barsony J.** 2002. Retinoid X receptor dominates the nuclear import and export of the unliganded vitamin D receptor. Mol. Endocrinol. **16:**1738–1751. http://dx.doi.org/10.1210/me.2001-0345.
30. **Feige JN, Gelman L, Tudor C, Engelborghs Y, Wahli W, Desvergne B.** 2005. Fluorescence imaging reveals the nuclear behavior of peroxisome proliferator-activated receptor/retinoid X receptor heterodimers in the absence and presence of ligand. J. Biol. Chem. **280:**17880–17890. http://dx.doi.org/10.1074/jbc.M500786200.
31. **Maruvada P, Baumann CT, Hager GL, Yen PM.** 2003. Dynamic shuttling and intranuclear mobility of nuclear hormone receptors. J. Biol. Chem. **278:**12425–12432. http://dx.doi.org/10.1074/jbc.M202752200.
32. **Tudor C, Feige JN, Pingali H, Lohray VB, Wahli W, Desvergne B, Engelborghs Y, Gelman L.** 2007. Association with coregulators is the major determinant governing peroxisome proliferator-activated receptor mobility in living cells. J. Biol. Chem. **282:**4417–4426. http://dx.doi.org/10.1074/jbc.M608172200.
33. **Schmiedeberg L, Weisshart K, Diekmann S, Meyer Zu Hoerste G, Hemmerich P.** 2004. High- and low-mobility populations of HP1 in heterochromatin of mammalian cells. Mol. Biol. Cell **15:**2819–2833. http://dx.doi.org/10.1091/mbc.E03-11-0827.

34. **Vamosi G, Baudendistel N, von der Lieth CW, Szaloki N, Mocsar G, Muller G, Brazda P, Waldeck W, Damjanovich S, Langowski J, Toth K.** 2008. Conformation of the c-Fos/c-Jun complex in vivo: a combined FRET, FCCS, and MD-modeling study. Biophys. J. **94:**2859–2868. http://dx.doi.org/10.1529/biophysj.107.120766.
35. **Baudendistel N, Muller G, Waldeck W, Angel P, Langowski J.** 2005. Two-hybrid fluorescence cross-correlation spectroscopy detects protein-protein interactions in vivo. Chemphyschem **6:**984–990. http://dx.doi.org/10.1002/cphc.200400639.
36. **Dross N, Spriet C, Zwerger M, Muller G, Waldeck W, Langowski J.** 2009. Mapping eGFP oligomer mobility in living cell nuclei. PLoS One **4:**e5041. http://dx.doi.org/10.1371/journal.pone.0005041.
37. **Wachsmuth M, Waldeck W, Langowski J.** 2000. Anomalous diffusion of fluorescent probes inside living cell nuclei investigated by spatially-resolved fluorescence correlation spectroscopy. J. Mol. Biol. **298:**677–689. http://dx.doi.org/10.1006/jmbi.2000.3692.
38. **Weiss M, Elsner M, Kartberg F, Nilsson T.** 2004. Anomalous subdiffusion is a measure for cytoplasmic crowding in living cells. Biophys. J. **87:**3518–3524. http://dx.doi.org/10.1529/biophysj.104.044263.
39. **Banks DS, Fradin C.** 2005. Anomalous diffusion of proteins due to molecular crowding. Biophys. J. **89:**2960–2971. http://dx.doi.org/10.1529/biophysj.104.051078.
40. **Buchholz J, Krieger JW, Mocsar G, Kreith B, Charbon E, Vamosi G, Kebschull U, Langowski J.** 2012. FPGA implementation of a 32x32 auto-correlator array for analysis of fast image series. Optics Express **20:**17767–17782. http://dx.doi.org/10.1364/OE.20.017767.
41. **Capoulade J, Wachsmuth M, Hufnagel L, Knop M.** 2011. Quantitative fluorescence imaging of protein diffusion and interaction in living cells. Nat. Biotechnol. **29:**835–839. http://dx.doi.org/10.1038/nbt.1928.
42. **Mocsar G, Kreith B, Buchholz J, Krieger JW, Langowski J, Vamosi G.** 2012. Multiplexed multiple-tau auto- and cross-correlators on a single field programmable gate array. Rev. Sci. Instrum. **83:**046101. http://dx.doi.org/10.1063/1.3700810.
43. **Wohland T, Shi X, Sankaran J, Stelzer EH.** 2010. Single plane illumination fluorescence correlation spectroscopy (SPIM-FCS) probes inhomogeneous three-dimensional environments. Optics Express **18:**10627–10641. http://dx.doi.org/10.1364/OE.18.010627.